Energy scale of nematic ordering in the parent iron-based superconductor $BaFe_2As_2$

Alexander Fedorov,[1,2] Alexander Yaresko,[3] Erik Haubold,[1] Yevhen Kushnirenko,[1] Timur Kim,[4] Bernd Büchner,[1] Saicharan Aswartham,[1] Sabine Wurmehl,[1] and Sergey Borisenko[1]

[1]*Leibniz Institute for Solid State and Materials Research IFW Dresden, D-01069 Dresden, Germany*
[2]*Helmholtz-Zentrum Berlin für Materialien und Energie, Albert-Einstein-Str. 15, 12489 Berlin, Germany*
[3]*Max Planck Institute for Solid State Research, Heisenbergstrasse 1, 70569 Stuttgart, Germany*
[4]*Diamond Light Source, Harwell Campus, Didcot OX11 0DE, United Kingdom*

(Received 30 October 2018; revised manuscript received 2 April 2019; published 24 July 2019)

Nematicity plays an important role in the physics of iron-based superconductors (IBS). Its microscopic origin and in particular its importance for the mechanism of high-temperature superconductivity itself are highly debated. A crucial knowledge in this regard is the degree to which the nematic order influences the electronic structure of these materials. Earlier angle-resolved photoemission spectroscopy (ARPES) studies found that the effect is dramatic in three families of IBS including 11, 111, and 122 compounds: Energy splitting reaches 70 meV and Fermi surface becomes noticeably distorted. More recent experiments, however, reported significantly lower energy scale in 11 and 111 families, thus questioning the degree and universality of the impact of nematicity on the electronic structure of IBS. Here, we revisit the electronic structure of the undoped parent $BaFe_2As_2$ (122 family). Our systematic ARPES study, including the detailed temperature and photon energy dependencies, points to the significantly smaller energy scale also in this family of materials, thus establishing the universal scale of this phenomenon in IBS. Our results form a necessary quantitative basis for theories of high-temperature superconductivity focused on the nematicity.

DOI: 10.1103/PhysRevB.100.024517

I. INTRODUCTION

Nematic order in iron-based superconductors (IBS) has been confirmed experimentally and seems to be an essential ingredient of superconductivity [1–4]. The transition from the tetragonal to orthorhombic phase is of electronic origin [1–6] and it is highly debated whether the striped magnetic or orbital ordering is directly responsible for this phenomenon [7,8].

In order to advance in this debate, it is necessary to provide quantitative theories with exact characterization of electronic nematicity. One of the quantitative estimates in terms of energy and momentum comes from angle-resolved photoemission [6,9–16]. The energy splitting was reported to reach 70 meV in $BaFe_2As_2$ (Ba122) [9], 40 meV in NaFeAs [16,17], and 60 meV in FeSe [6,9–15]. Such a strong modification of the electronic structure could reveal the dominant interactions which are able to drive the pairing in IBS. However, later revisits of the electronic structures of some of the main stoichiometric members of the IBS family, FeSe and NaFeAs, suggested that the energy scale corresponding to the nematic ordering has to be scaled down [5,18,19]. The energy scale was reported to be significantly smaller than believed earlier, of the order of 10–15 meV. In contrast, recent re-evaluation of data on strained and/or detwinned Ba122 and FeSe crystals rescale nematic energy up to 100 [20] and 50 meV [21,22].

Since the very first evidence from the ARPES measurements of the archetypal $BaFe_2As_2$ systems [9,23], it has been highly desirable to establish the energy and momentum scale also in this key family of IBS materials. Moreover, previous ARPES studies of Ba122 [23–27] did not converge to a common picture. The discrepancies are mostly related to three dimensionality, nesting conditions, and disagreement with the band-structure calculations and bulk sensitive de Haas-van Alphen (dHvA) experiments [28,29]. Several experiments have been carried out on the detwinned samples [9,20,30]. Again, the conclusions drawn in these studies are controversial. Kim *et al.* [30] found a good agreement with the band-structure calculations, whereas Yi *et al.* [9] detected an unbalanced occupation of the d_{xz} and d_{yz} orbitals which develops fully at the transition temperature. Such different estimations of the amplitude of nematic splitting in the literature potentially stem from the comparison of the electronic structure of the modified ("detwinned" does not necessarily mean already not "strained") samples with arbitrary approximations to the band-structure calculations (tight-binding fits). Indeed, compressive strain has significant impact on the electronic structure of IBS [31] and opens a new avenue for experimental and theoretical studies.

In this study, we revisit the electronic structure of the stoichiometric parent Ba122 compound. We use high-resolution ARPES and conventional band-structure calculations in order to understand the fine details of the low-energy electron dynamics and its evolution in a broad temperature interval. A step-by-step analysis of the influence of the three-dimensionality and nematic and spin-density wave (SDW) transitions on the electronic structure of Ba122 allowed us to single out the optimal conditions for the experiment which directly provides the quantitative estimate of the energy and momentum scales related to the nematicity in this basic but important material.

II. EXPERIMENTAL AND COMPUTATIONAL DETAILS

A. Experimental details

High-quality single crystals of $BaFe_2As_2$ were grown by the self-flux technique and were characterized by several complementary methods as described in Ref. [32]. Ba122 exhibits stripe-type anteferromagnetic ordering of Fe spins below the Neel temperature ≈ 140 K, accompanied by a structural phase transition. The high-temperature paramagnetic tetragonal structure has lattice parameters $a = b = 3.9625$ Å, $c = 13.0168$ Å while the orthorombic phase has $a = 5.6146$ Å, $b = 5.5742$ Å, $c = 12.9453$ Å [33]. Neutron diffraction studies have shown that the magnetic modulation vector is $Q = (1, 0, 1)$ in the above orthorhombic setting, with the spin orientation parallel to a [34].

ARPES measurements were performed at the I05 beamline of Diamond Light Source, UK [35]. Single-crystal samples were cleaved *in situ* in a vacuum lower than 2×10^{-10} mbar and measured at temperatures ranging from 5.7 to 270 K. Measurements were performed using linear horizontal (LH) and linear vertical (LV) polarized synchrotron light with variable photon energy, utilizing Scienta R4000 hemispherical electron energy analyzer with an angular resolution of 0.1 deg and an energy resolution of 3 meV.

B. Computational details

Self-consistent band-structure calculations were performed using the linear muffin-tin orbital (LMTO) method [36] in the atomic sphere approximation (ASA) as implemented in PY LMTO computer code [37]. The Perdew-Wang parametrization [38] was used to construct the exchange correlation potential in the local density approximation (LDA). Spin-orbit coupling (SOC) was taken into account at the variational step.

The Fe magnetic moment of 1.24 μ_B calculated using the Perdew-Wang parametrization of the LSDA exchange-correlation potential is indeed larger than the experimental ordered moment of 0.8–0.9 μ_B. On the other hand, DFT calculations reproduce correct stripelike magnetic ground state with shrinking of the lattice along ferromagnetic (FM) and its expansion along antiferromagnetic (AF) Fe-Fe bonds. Even such a subtle effect as alignment of the Fe moments along the direction of AF Fe chains is captured by DFT calculations when spin-orbit coupling is taken into account.

III. RESULTS AND DISCUSSION

Taking into account all previous measurements and controversies, we first present the data recorded at low temperatures, deep in the magnetic phase, and compare them with the corresponding band-structure calculations integrated along $\vec{k}_z$ in Fig. 1. The recorded Fermi surface in Fig. 1(a) consists of three pockets with the holelike one in the center and two other electron-like ones. The projection of the theoretical Fermi surface on $\vec{k}_x$-$\vec{k}_y$ plane [Fig. 1(d)] is in a striking agreement with the experimental Fermi surface map. All features seen in the experiment are qualitatively reproduced by the band-structure calculations, namely the big holelike structure in the center, four big electron-like pockets, and four holelike small pockets which appear to be inside the electron-like ones. The sizes and exact shapes of all pockets are not in a perfect agreement because of the so-called red-blue shift that we discuss in detail later. Now we compare our results with the dHvA measurements [29]. Taking into account that we observed signals from two rotational domains simultaneously, we designate our center pocket as α, four big electron pockets as δ, and four tiny inlay pockets as γ, respectively. Integrating the corresponding areas enclosed by the recorded Fermi

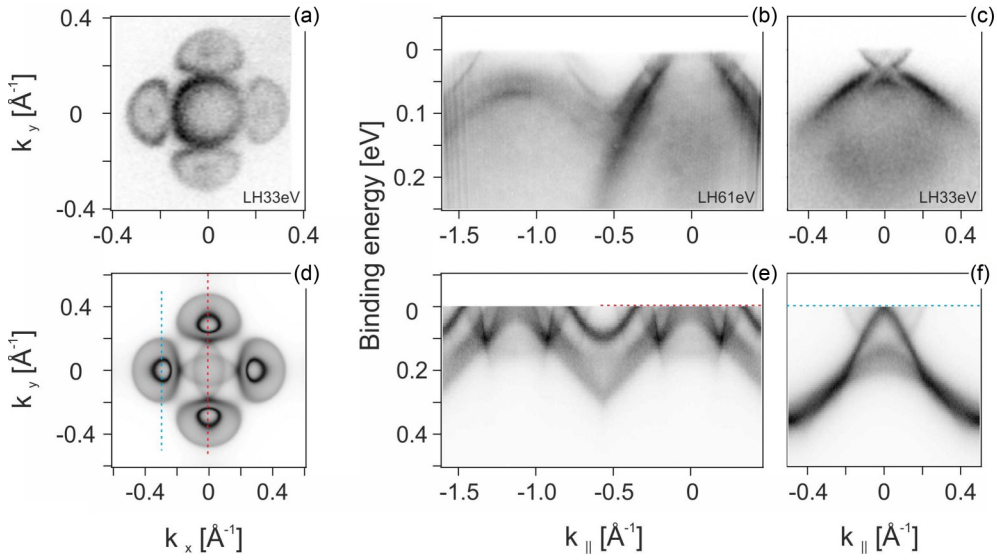

FIG. 1. ARPES data accompanied by corresponding DFT calculated band stucture in the SDW phase without SOC and fully integrated over $\vec{k}_z$ in the presence of two rotational domains: [(a), (d)] Fermi surface in SDW phase. [(b), (e)] Cut along the Γ-M direction. [(c), (f)] Cut along the cyan dashed line. Only those bands which cross the E_f are shown in DFT data. Nearly vertical stripy patterns visible at the edges of panel (b) are caused by interference of electrons on the analyzer slit and do not modify significantly observed energy or momentum distributions of the intensity.

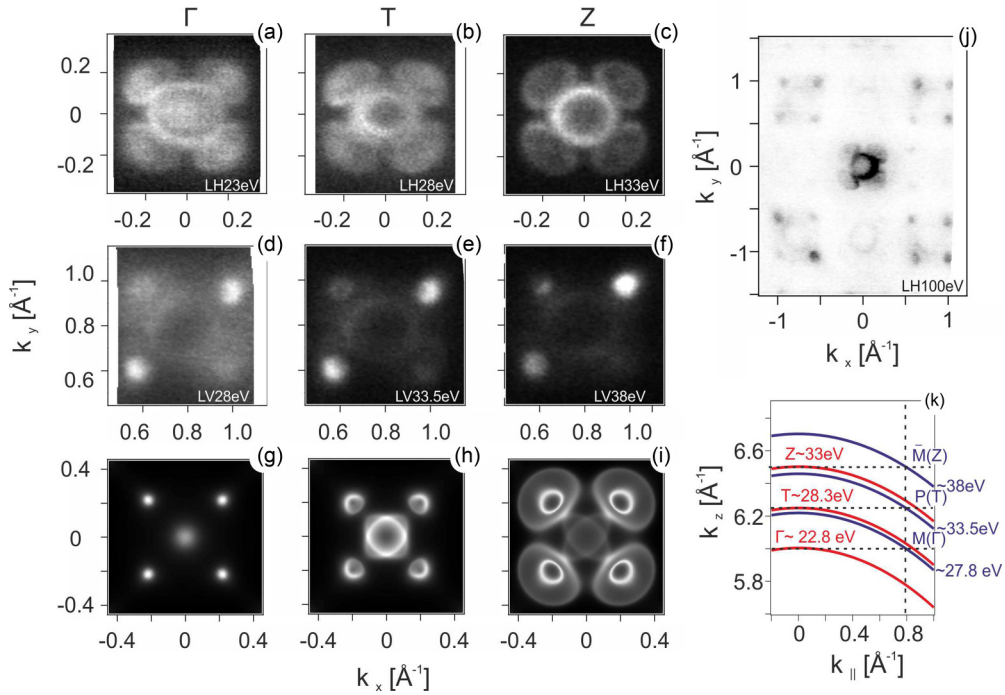

FIG. 2. (a)–(f) ARPES derived Fermi surfaces recorded at different photon energies corresponding to the high-symmetry point in the BZ. (g)–(i) Calculated Fermi surfaces in the corresponding high-symmetry points of the BZ integrated over the quarter in $\vec{k}_z$ direction. (j) Overview FS map recorded at 100-eV photon energy. (k) $\vec{k}_z$ vs $\vec{k}_{||}$ relations.

surface, we estimate corresponding frequencies as $F_\alpha \approx 515$ T, $F_\delta \approx 440$ T and $F_\gamma \approx 50$ T, which is in good agreement with the measured values. The progress in the data quality could be best seen by comparison of this map with our previous study [27]. Similar to the previously reported picture [9], we observe additional intensity inside the α pocket at other photon energies, which is indeed absent in dHvA measurements. We attribute this intensity to the integration over a certain portion in k_z direction, as we discuss later.

The underlying dispersions are compared in Fig. 1. Also, here one can notice a remarkable correspondence of the calculated dispersions with the experimental ones. Basically, all the states predicted by the mean field theory can be identified in experimental data, at least on a qualitative level. In order to achieve a quantitative agreement, one needs to take into account several known modifications. These are the global bandwidth renormalization, the relative energy shift between hole and electron pockets in the tetragonal state (blue-red shifts) [5,39,40], and matrix element effects which govern the intensities of the particular features. In order to reproduce size of the small electron pocket γ, calculated Fermi energy has to be lowered. The shift down of 50 meV brought the intense "V" -like crossings (at 50–70 meV) closer to the Fermi level [Fig. 1(f)], as in the experiment [Fig. 1(c)]. The controversial doublet feature at 50- to 70-meV binding energy [30] is now also reproduced by the calculations. The size of the central hole pocket α and of the big electron pockets δ can be tuned simultaneously. We found the best correspondence up-shifting the Fermi level by only 25 meV. Because the blue-red shifts are present in the tetragonal phase, a single rigid shift of the band structure would not be sufficient in a folded magnetic state, in order to reproduce all features originally related to hole- and electron-like pockets simultaneously.

Based on a reasonably good correspondence between the experiment and the band-structure calculations in Fig. 1, two questions rise: (i) Is the full integration over $\vec{k}_z$ essential? (ii) Where is the strong influence of the nematic energy scale of the order of 70 meV? To answer the first question, we have carried out extensive ARPES experiments to study the $\vec{k}_z$ dependence of the electronic structure. The usual way to perform such a study is to vary photon energy of excitation light and thus the full momentum $\vec{k}$ of the emitted electron becomes controlled. Notably, using photons in ultraviolet range suitable for high-resolution ARPES leads to relatively small $\vec{k}$ values. Therefore, $\vec{k}_z$ projection becomes very sensitive to an emission angle, i.e., corresponding $\vec{k}_{||}$. We demonstrate this fact in Fig. 2(k) together with optimized photon energy values corresponding to different high-symmetry points in the Brillouin zone (BZ). We have identified these points considering extensive photon energy-dependent measurements, which are in a good agreement with previously reported values [25]. (See the Supplemental Material [41] for the corresponding photon energy scan.)

We present the data in the SDW regime taken in different high-symmetry points of the BZ in the center of each shown map in Figs. 2(a)–2(f) as well as the large overview FS map in Fig. 2(g) recorded at 100 eV photon energy. In the mean field theory, the maps in the upper row of experimental data should be equivalent to the ones from the lower row. However, it is known that even without influence of the matrix elements, the photocurrent strongly depends on the degree of the potential

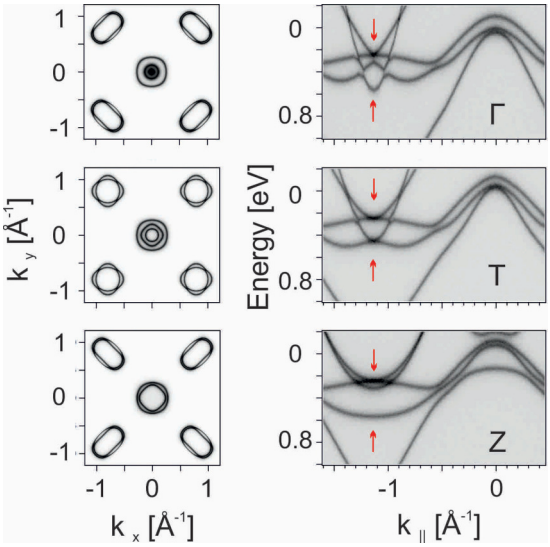

FIG. 3. Band structure calculated in the tetragonal phase for three high-symmetry planes in the BZ.

modulations in the density wave state [42]. That is why the intensity distribution in the corner of tetragonal BZ at all $\vec{k}_z$ values are different from the ones in the center of the BZ. In particular, the four smallest Fermi surfaces are always brighter in the second row of panels while the central rounded ones and the larger deformed ellipses adjacent to it are more clearly visible in the upper row. In Figs. 2(h)–2(j), we show for comparison the theoretical cuts through the FS now integrated in the smaller $\vec{k}_z$ interval (0.25 BZ). As seen from Fig. 2, while the general $\vec{k}_z$ evolution can be tracked in the experimental data, there is always a certain admixture of the signal from different $\vec{k}_z$ values. This indicates that the $\vec{k}_z$ selectivity of this particular experiment is not very high, probably implying the smaller electron escape depth and thus lower $\vec{k}_z$ resolution. Practically, however, the intensity distribution changes when switching from map to map, indicating the possibility of finding the conditions optimal for the observation of only the desired $\vec{k}_z$ portion of the BZ. For instance, the maps centered at nonzero momentum do not have a strong signal contribution from the big holelike pocket. This is because the modulating potential of SDW is not strong enough to make the corner and the center of the tetragonal BZ equivalent. As in the cases of FeSe [5,18] and NaFeAs [19], the calculations suggest that the most convenient set of features to determine the energy scale of nematic order are the dispersions which support the FS in the corner of the tetragonal BZ. However, because Ba122 has a double-layer structure, there is an important difference overlooked earlier.

In Fig. 3, we show the results of the band-structure calculations in the tetragonal phase. First of all, band-structure calculations imply significant $\vec{k}_z$ dispersion and this fact alone actually prohibits the comparison of the data taken using the single-photon energy along the diagonal cut with the calculated result for constant $\vec{k}_z$ value: Going away from the center of the BZ, the probed $\vec{k}_z$ values will constantly decrease and upon reaching the corner of the BZ will correspond to completely different values [see Fig. 2(k)]. The most convenient place to track the influence of the nematicity on the electronic structure in Ba122 is at the corner of the BZ where the electron-like dispersions have their bottoms and spin-orbit splitting is zero [43]. The tops of holelike bands are not occupied and there is admixture of the spin-orbit splitting [39]. Moreover, the data presented in Fig. 3 clearly show that the most suitable for this purpose is the TNP plane, where the energy distribution is expected to have only two peaks. Therefore, a minimal number of peaks (four) are expected in the nematic state, closely following the dispersion in 11 and 111 compounds [5,18,19].

Now we can switch to high-temperature measurements and see what exactly happens at the transition in Fig. 4. We start with overview maps recorded with 100-eV photon energy slightly above and below transition. From the first glance, we cannot identify any significant changes between corresponding maps and traces of the folded band structure visible on the low-temperature map in Fig. 2. Thus, we can conclude that just below transition the influence of the magnetic modulations is still weak in ARPES and most changes correspond to the accompanying structural transition. Now, we turn to the underlying dispersions of electron pocket. In analogy with FeSe [5], we performed diagonal T-N cuts (Fig. 4) and corresponding DFT calculations for tetragonal phase (Fig. 4) and orthorhombic phase with two domains (Fig. 4). Similarly, we expect to observe evolution in the corresponding energy distribution curve (EDC) in the corner of the BZ from two to four features. However, experimental observation of the four features' structures is difficult even down to 10 K (Fig. 4) because of higher broadening caused by self-energy and moderate resolution in the $\vec{k}_z$ direction. Indeed, we always observe two peaks separated by 70 meV, which we attribute to the two orbitals: $d_{xz/yz}$ and d_{xy}. Previously, these two states were not resolvable at high temperature [9] and evolution from the single to double feature was assigned to the nematic transition. Here, we observe that these states are an essential component of the band structure, which is now fully in agreement with corresponding DFT calculations.

Since analysis of EDC is complicated, we switched to corresponding momentum distribution curve (MDC) cuts at the Fermi energy. In the tetragonal phase, we expect four peaks corresponding to two electron pockets. Below the orthorhombic transition and in the presence of two domains, we expect twice as many features. In experimental data above the transition temperature, we observe MDC, which can be well fitted by four Lorentzian peaks (Fig. 4). Slightly below the transition, we observe significant broadening of the corresponding MDC. We used two sets of four peaks with same parameters as in the tetragonal case to describe the low-temperature MDC. From our fit, we estimate the magnitude of nematic splitting in momentum of about $0.07\,\text{Å}^{-1}$. Using an average dispersion relation (i.e., Fermi velocity) of about $0.3\,\text{eV}/\text{Å}^{-1}$, we estimate the nematic energy scale to be of the order of 20 meV.

The difficulty of determining the degree to which nematic order changes the electronic structure in Ba122 is that it sets in simultaneously with the SDW order. This is because the magnetic order folds the bands and opens the significant interaction gaps. However, our data presented above suggest

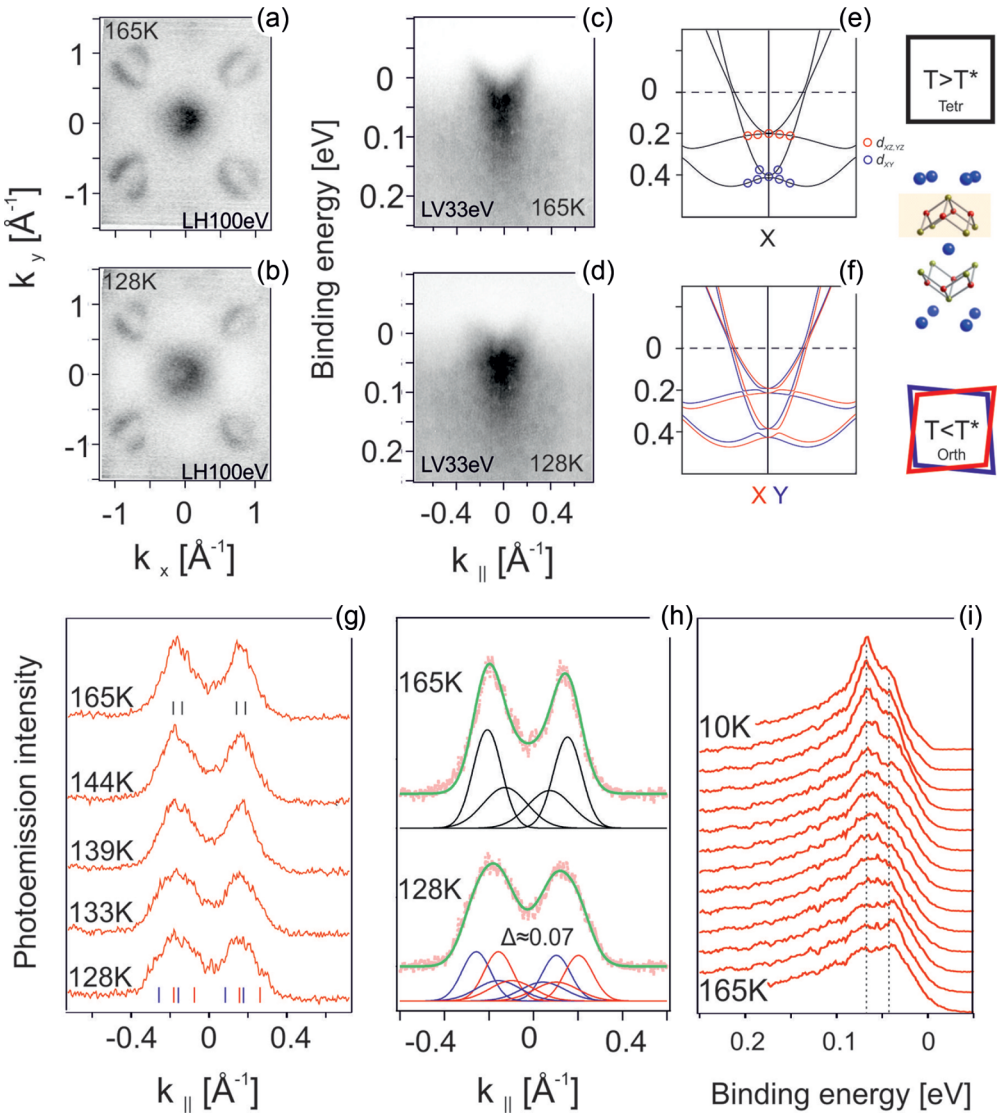

FIG. 4. [(a), (b)] Overview ARPES maps recorded at 100-eV photon energy above and below Tc. [(c), (d)] High-resolution ARPES data recorded in the T-N direction above and below Tc. [(e), (f)] corresponding DFT calculations in tetragonal and orthorombic phases. (g) Temperature evolution of MDC cut taken on the Fermi energy corresponding to panel (c). (h) Fit results of MDC curves above and below Tc. (i) Temperature evolution of EDC curve taken in the corner of the BZ.

that the particular experimental conditions allow us to see the portions of the momentum space where the folded replicas are weak and the consequences of the structural transition can be estimated separately. In analogy with FeSe and NaFeAs, one can do this at the corner of the tetragonal BZ watching the bottoms of the electron-like pockets, with the important difference that this can be done only for a particular $\vec{k}_z$ interval, namely near the P point of the BZ. As we have shown above, this is not straightforward since a considerable admixture of the signal from other $\vec{k}_z$ values is observed. This latter observation explains why the previous studies did not reach a consensus as regards the exact $\vec{k}_z$ dependence. Moreover, we have not detected a significant unbalanced occupation of the d_{xz} and d_{yz} orbitals at the transition temperature and nearly 40 K below it. At still lower temperatures, the folded SDW replicas prohibit further tracking of the features related to nematic order alone. In principle, our extracted values of nematic energy and momentum scales can already be concluded from the fact that the conventional magnetic calculations fully describe the electronic structure observed experimentally at low temperatures. Our results thus establish the universality of the strength of nematic ordering in the iron-based superconductors and provide the quantitative basis for the theories of high-temperature superconductivity in iron-based materials.

IV. CONCLUSIONS

We revisited the electronic structure of the stoichiometric parent Ba122 using high-resolution ARPES and conventional band-structure calculations. We demonstrated that general features of the band structure in the SDW phase are well described by magnetic DFT calculations. Our calculations reveal significant $\vec{k}_z$ dispersion in this compound and

experimental data show moderate $\vec{k}_z$ resolution causing additional energy and momentum broadening. Optimizing experimental conditions we were able to detect band-structure modification crossing the critical temperature and quantitative estimate the energy scale of 20 meV related to the nematicity.

ACKNOWLEDGMENTS

We are grateful to A. Chubukov, M. Watson, P. Hirschfeld, R. Valenti, S. Roessler, I. Eremin, and S.-H. Baek for the fruitful discussions. This work has been supported by Deutsche Forschungsgemeinschaft (DFG) through the Priority Programme SPP1458 (Grant No. BU887/15-1 and No. BO1912/6-1), through Grant No. DFG-GRK1621, and through the Emmy Noether Programme WU595/3-3 (S.W.). We acknowledge Diamond Light Source for access to beamline I05 (Proposals No. SI13856-1 and No. SI15936-1) that contributed to the results presented here. A.F., T.K., Y.K., E.H., and S.B. conceived the experiments. DFT calculations were performed by A.Y. The high-quality $BaFe_2As_2$ crystals were grown by S.A. and S.W. The data were discussed with B.B. The paper was written by A.F and S.B. All authors have read and approved the decisive version of the paper. The authors declare no competing financial interests.

[1] R. M. Fernandes, A. V. Chubukov, and J. Schmalian, Nat. Phys. **10**, 97 (2014).
[2] J. Li, P. J. Pereira, J. Yuan, Y.-Y. Lv, M.-P. Jiang, D. Lu, Z.-Q. Lin, Y.-J. Liu, J.-F. Wang, L. Li, X. Ke, G. Van Tendeloo, M.-Y. Li, H.-L. Feng, T. Hatano, H.-B. Wang, P.-H. Wu, K. Yamaura, E. Takayama-Muromachi, J. Vanacken, L. F. Chibotaru, and V. V. Moshchalkov, Nat. Commun. **8**, 1880 (2017).
[3] A. Chubukov and P. Hirschfeld, Phys. Today **68**(6), 46 (2015).
[4] A. Kreisel, B. M. Andersen, P. O. Sprau, A. Kostin, J. C. S. Davis, and P. J. Hirschfeld, Phys. Rev. B **95**, 174504 (2017).
[5] A. Fedorov, A. Yaresko, T. K. Kim, Y. Kushnirenko, E. Haubold, T. Wolf, M. Hoesch, A. Grüneis, B. Büchner, and S. V. Borisenko, Sci. Rep. **6**, 1 (2016).
[6] M. D. Watson, T. K. Kim, A. A. Haghighirad, N. R. Davies, A. McCollam, A. Narayanan, S. F. Blake, Y. L. Chen, S. Ghannadzadeh, A. J. Schofield, M. Hoesch, C. Meingast, T. Wolf, and A. I. Coldea, Phys. Rev. B **91**, 155106 (2015).
[7] A. V. Chubukov, M. Khodas, and R. M. Fernandes, Phys. Rev. X **6**, 041045 (2016).
[8] S.-H. Baek, D. V. Efremov, J. M. Ok, J. S. Kim, J. van den Brink, and B. Büchner, Nat. Mater. **14**, 210 (2014).
[9] M. Yi, D. Lu, J.-H. Chu, J. G. Analytis, A. P. Sorini, A. F. Kemper, B. Moritz, S.-K. Mo, R. G. Moore, M. Hashimoto, W.-S. Lee, Z. Hussain, T. P. Devereaux, I. R. Fisher, and Z.-X. Shen, Proc. Natl. Acad. Sci. USA **108**, 6878 (2011).
[10] T. Shimojima, Y. Suzuki, T. Sonobe, A. Nakamura, M. Sakano, J. Omachi, K. Yoshioka, M. Kuwata-Gonokami, K. Ono, H. Kumigashira, A. E. Böhmer, F. Hardy, T. Wolf, C. Meingast, H. V. Löhneysen, H. Ikeda, and K. Ishizaka, Phys. Rev. B **90**, 121111 (2014).
[11] K. Nakayama, Y. Miyata, G. N. Phan, T. Sato, Y. Tanabe, T. Urata, K. Tanigaki, and T. Takahashi, Phys. Rev. Lett. **113**, 237001 (2014).
[12] P. Zhang, T. Qian, P. Richard, X. P. Wang, H. Miao, B. Q. Lv, B. B. Fu, T. Wolf, C. Meingast, X. X. Wu, Z. Q. Wang, J. P. Hu, and H. Ding, Phys. Rev. B **91**, 214503 (2015).
[13] L. Fanfarillo, J. Mansart, P. Toulemonde, H. Cercellier, P. L. Fevre, F. Bertran, B. Valenzuela, L. Benfatto, and V. Brouet, Phys. Rev. B **94**, 155138 (2016).
[14] H. C. Xu, X. H. Niu, D. F. Xu, J. Jiang, Q. Yao, M. Abdel-Hafiez, D. A. Chareev, A. N. Vasiliev, R. Peng, and D. L. Feng, Phys. Rev. Lett. **117**, 157003 (2016).
[15] Z. R. Ye, C. F. Zhang, H. L. Ning, W. Li, L. Chen, T. Jia, M. Hashimoto, D. H. Lu, Z. X. Shen, and Y. Zhang, arXiv:1512.02526.
[16] M. Yi, D. H. Lu, R. G. Moore, K. Kihou, C.-H. Lee, A. Iyo, H. Eisaki, T. Yoshida, A. Fujimori, and Z.-X. Shen, New J. Phys. **14**, 073019 (2012).
[17] Y. Zhang, C. He, Z. R. Ye, J. Jiang, F. Chen, M. Xu, Q. Q. Ge, B. P. Xie, J. Wei, M. Aeschlimann, X. Y. Cui, M. Shi, J. P. Hu, and D. L. Feng, Phys. Rev. B **85**, 085121 (2012).
[18] M. D. Watson, T. K. Kim, L. C. Rhodes, M. Eschrig, M. Hoesch, A. A. Haghighirad, and A. I. Coldea, Phys. Rev. B **94**, 201107(R) (2016).
[19] M. D. Watson, S. Aswartham, L. C. Rhodes, B. Parrett, H. Iwasawa, M. Hoesch, I. Morozov, B. Büchner, and T. K. Kim, Phys. Rev. B **97**, 035134 (2018).
[20] H. Pfau, C. R. Rotundu, J. C. Palmstrom, S. D. Chen, M. Hashimoto, D. Lu, A. F. Kemper, I. R. Fisher, and Z.-X. Shen, Phys. Rev. B **99**, 035118 (2019).
[21] M. Yi, Y. Zhang, H. Pfau, T. Chen, Z. Ye, M. Hashimoto, R. Yu, Q. Si, D.-H. Lee, P. Dai, Z. X. Shen, D. Luan, and R. J. Birgeneau, arXiv:1903.04557.
[22] S. Huh, J. Seo, B. Kim, S. Cho, J. Jung, S. Kim, Y. Koh, C. Kwon, J. Kim, W. Kyung, J. D. Denlinger, Y. Kim, B. Chae, N. Kim, Y. Kim, and C. Kim, arXiv:1903.08360.
[23] M. Yi, D. H. Lu, J. G. Analytis, J.-H. Chu, S.-K. Mo, R.-H. He, M. Hashimoto, R. G. Moore, I. I. Mazin, D. J. Singh, Z. Hussain, I. R. Fisher, and Z.-X. Shen, Phys. Rev. B **80**, 174510 (2009).
[24] T. Shimojima, K. Ishizaka, Y. Ishida, N. Katayama, K. Ohgushi, T. Kiss, M. Okawa, T. Togashi, X.-Y. Wang, C.-T. Chen, S. Watanabe, R. Kadota, T. Oguchi, A. Chainani, and S. Shin, Phys. Rev. Lett. **104**, 057002 (2010).
[25] T. Kondo, R. M. Fernandes, R. Khasanov, C. Liu, A. D. Palczewski, N. Ni, M. Shi, A. Bostwick, E. Rotenberg, J. Schmalian, S. L. Bud'ko, P. C. Canfield, and A. Kaminski, Phys. Rev. B **81**, 060507(R) (2010).
[26] Y. Nakashima, A. Ino, S. Nagato, H. Anzai, H. Iwasawa, Y. Utsumi, H. Sato, M. Arita, H. Namatame, M. Taniguchi, T. Oguchi, Y. Aiura, I. Hase, K. Kihou, C. Lee, A. Iyo, and H. Eisaki, Solid State Commun. **157**, 16 (2013).
[27] V. B. Zabolotnyy, D. S. Inosov, D. V. Evtushinsky, A. Koitzsch, A. A. Kordyuk, G. L. Sun, J. T. Park, D. Haug, V. Hinkov, A. V. Boris, C. T. Lin, M. Knupfer, A. N. Yaresko, B. Büchner, A. Varykhalov, R. Follath, and S. V. Borisenko, Nature (London) **457**, 569 (2009).
[28] J. G. Analytis, R. D. McDonald, J.-H. Chu, S. C. Riggs, A. F. Bangura, C. Kucharczyk, M. Johannes, and I. R. Fisher, Phys. Rev. B **80**, 064507 (2009).

[29] T. Terashima, N. Kurita, M. Tomita, K. Kihou, C.-H. Lee, Y. Tomioka, T. Ito, A. Iyo, H. Eisaki, T. Liang, M. Nakajima, S. Ishida, S.-i. Uchida, H. Harima, and S. Uji, Phys. Rev. Lett. **107**, 176402 (2011).

[30] Y. Kim, H. Oh, C. Kim, D. Song, W. Jung, B. Kim, H. J. Choi, C. Kim, B. Lee, S. Khim, H. Kim, K. Kim, J. Hong, and Y. Kwon, Phys. Rev. B **83**, 064509 (2011).

[31] G. N. Phan, K. Nakayama, K. Sugawara, T. Sato, T. Urata, Y. Tanabe, K. Tanigaki, F. Nabeshima, Y. Imai, A. Maeda, and T. Takahashi, Phys. Rev. B **95**, 224507 (2017).

[32] S. Aswartham, C. Nacke, G. Friemel, N. Leps, S. Wurmehl, N. Wizent, C. Hess, R. Klingeler, G. Behr, S. Singh, and B. Büchner, J. Crystal Growth **314**, 341 (2011).

[33] M. Rotter, M. Tegel, D. Johrendt, I. Schellenberg, W. Hermes, and R. Pöttgen, Phys. Rev. B **78**, 020503(R) (2008).

[34] Q. Huang, Y. Qiu, W. Bao, M. A. Green, J. W. Lynn, Y. C. Gasparovic, T. Wu, G. Wu, and X. H. Chen, Phys. Rev. Lett. **101**, 257003 (2008).

[35] M. Hoesch, T. K. Kim, P. Dudin, H. Wang, S. Scott, P. Harris, S. Patel, M. Matthews, D. Hawkins, S. G. Alcock, T. Richter, J. J. Mudd, M. Basham, L. Pratt, P. Leicester, E. C. Longhi, A. Tamai, and F. Baumberger, Rev. Sci. Instruments **88**, 013106 (2017).

[36] O. K. Andersen, Phys. Rev. B **12**, 3060 (1975).

[37] V. Antonov, B. Harmon, and A. Yaresko, *Electronic Structure and Magneto-optical Properties of Solids* (Kluwer, Dordrecht, 2004).

[38] J. P. Perdew and Y. Wang, Phys. Rev. B **45**, 13244 (1992).

[39] S. V. Borisenko, D. V. Evtushinsky, Z.-H. Liu, I. Morozov, R. Kappenberger, S. Wurmehl, B. Buchner, A. N. Yaresko, T. K. Kim, M. Hoesch, T. Wolf, and N. D. Zhigadlo, Nat. Phys. **12**, 311 (2016).

[40] Y. S. Kushnirenko, A. A. Kordyuk, A. V. Fedorov, E. Haubold, T. Wolf, B. Büchner, and S. V. Borisenko, Phys. Rev. B **96**, 100504(R) (2017).

[41] See Supplemental Material at http://link.aps.org/supplemental/10.1103/PhysRevB.100.024517 for the photon energy scan through the center of the surface Brillouin zone and determination of the high-symmetry points in the kz direction.

[42] V. B. Zabolotnyy, A. A. Kordyuk, D. S. Inosov, D. V. Evtushinsky, R. Schuster, B. Büchner, N. Wizent, G. Behr, S. Pyon, T. Takayama, H. Takagi, R. Follath, and S. V. Borisenko, Europhys. Lett. **86**, 47005 (2009).

[43] R. M. Fernandes and O. Vafek, Phys. Rev. B **90**, 214514 (2014).